Modelling the induction error in the Bøckman method for measuring furnace hearth voltages

by M. Sparta, V.K. Risinggård, U. Thisted

Affiliation:
NORCE Research, Universitetsveien 19, 4630 Kristiansand, Norway

Correspondence to:
V.K. Risinggård

Email:
veri@norceresearch.no

Dates:
Received: 27 Jun. 2025
Revised: .4 Apr. 2026
Accepted: 26 Jun. 2026
Published: Aug. 2026

How to cite:
Sparta M., Risinggård V.K., Thisted U. 2026. Modelling the induction error in the Bøckman method for measuring furnace hearth voltages. *Journal of the Southern African Institute of Mining and Metallurgy*, vol. 126, no. 8, pp. 475 – 482

DOI ID:
https://doi.org/10.17159/2411-9717/3761/2026

ORCiD:
M. Sparta
https://orcid.org/0000-0003-4218-5229
V.K. Risinggård
https://orcid.org/0000-0002-4841-6027
U. Thisted
https://orcid.org/0009-0008-3158-7402

Abstract

The Bøckman method is regularly used to obtain accurate measurements of the hearth voltage of smelting furnaces. The method uses three measuring leads in order to cancel induction errors using destructive interference when transferring the hearth voltage from the bottom of the furnace to the top of the electrodes. This paper presents an investigation of the Bøckman system's reliability, limitations, and background using finite-element-method simulations. A 3D model of an industrial-scale smelting furnace for Mn-alloy production is developed and used to examine the induction caused by balanced and unbalanced electrical conditions and material distributions.

Keywords

Submerged-arc furnace, electrode, induction, Bøckman method, finite-element method, mathematical modelling

Introduction

To ensure optimal operation of a large three-phase electric smelting furnace, accurate measurements of electrode loads are necessary (Magnussen, 2018). Typically, the electrode powers are calculated based on measurements of the electrode currents and the voltage drop between the top of the electrodes and the hearth of the furnace. For this purpose, the hearth of the furnace has to be electrically connected to transfer its potential to a measurement device in the control room. However, this poses significant problems as induced voltages due to the large magnetic field around the furnace lead to faulty readings (Stewart, 1980). Gerritsen et al. (2015) estimated that a furnace operating at 120 kA could see a 16 V error due to the induction when using a single measurement lead.

To circumvent this problem, Bøckman (1973a) proposed a method that uses three measuring leads. All leads are connected to the same point beneath the furnace, and each lead is drawn up to the top of the furnace directly outside one of the three electrodes. These three leads are connected in an area of low magnetic flux located above the furnace. The induced voltages in the leads interfere destructively; thus the voltage at the connection of the three leads replicates the voltage in the hearth. In the industry, it is widely believed that this method of measuring voltage between an electrode and the furnace hearth is, in principle, accurate. However, practical considerations often prevent a symmetric placement of the leads as described in the original patents (Bøckman, 1973a, 1973b). Moreover, it is unclear how well a method that depends on destructive interference of the induced voltages works for furnaces with asymmetrical electrical conditions.

There is no public survey available that analyses the background of the Bøckman approach and that discusses its reliability and limitations. To address this gap in the literature, this paper analyses different lead arrangements and their susceptibility to induction errors through computational investigations. Moreover, the effect of the electrical state of the furnace on the accuracy of the readings is examined. A finite-element-method (FEM) model (Zienkiewicz, Morgan, 2006) of an industrial-scale furnace for the production of ferromanganese was implemented to this end. The model builds on previous work on three-dimensional (3D) case studies of large submerged arc furnaces (Herland et al., 2018, 2019; Fromreide et al., 2021, 2023; Sparta, Varagnolo, Stråbø, et al., 2021; Sparta, Varagnolo, Martens, et al., 2021).

The use of 3D models for submerged-arc furnaces (SAF) has been discussed by several authors. For example, Dhainaut (2004) employed a DC model to examine the distribution of current and power when the current enters one electrode and evenly distributes to the other two electrodes. Halvorsen et al. (2016) demonstrated that, as long as electromagnetic induction can be disregarded, combining the results from two DC computations can determine the conditions at any point in the AC cycle or the time-averaged distribution of power and current. Bezuidenhout et al. (2009) developed a 3D computational fluid dynamics model to investigate the internal dynamics of an electrical furnace used for smelting platinum group metal concentrates. Scheepers et al. (2010) modelled and optimised a SAF for the production of phosphorus. Toh et al. (2005) utilised Maxwell's equations along with a finite-volume-method approach to model the steel-making process. Darmana et al. (2012) developed a multiphysics model incorporating thermodynamics, electricity, hydrodynamics, heat radiation, and chemical reactions for a SAF. Karalis et al. (2016) and Karalis et al. (2021) investigated the impact of slag properties, electrode shape and immersion depth on furnace heating in ferronickel processing. Yu et al. (2021) and Yu et al. (2023) developed a transient multiphysics model to predict the complex smelting state in a ferrochrome SAF. Finally, researchers at Reykjavík University simulated the effects of electrode shape, pitch circle diameter, and frequency on the current distribution in submerged arc furnaces for silicon production (Tesfahunegn, Magnússon, et al., 2018a, 2018b, 2020b, 2020a, 2021; Tesfahunegn, Sævarsdóttir, et al., 2018).

The paper is organised as follows: Section 2 presents a FEM model of a submerged arc furnace and outlines the approach to computing the inductive terms in the leads. Section 3 discusses the general properties of the induced terms. Section 4 investigates the phenomenon of destructive interference of the induced terms on symmetrically arranged leads under ideal furnace conditions, as well as the impact of breaking the lead symmetry. Finally, Sections 5 and 6 extends the analysis to the case of an unbalanced furnace.

Finite-element model

As shown in Figure 1 (left panel), the furnace model is 12.3 m in diameter and approximately 9 m high to the top of the roof and includes three electrodes, each with a diameter of 1.8 m spaced at 4.2 m apart (center-to-center distance). The furnace is composed of a steel roof and shell with a thickness of 25 mm, as well as non-conductive insulation layers (200 mm), conductive carbon materials (ranging from 660 mm to 850 mm thickness and extending up to 5 m above the alloy layer), charge banks between the electrodes with varying electrical properties (resistivity ranging from 10 mΩ·m to 300 mΩ·m), and coke beds. The coke beds have a range of diameters, from 4.86 m at the bottom to 2.16 m at the top, and a height of 1.53 m measured from the alloy layer. The shape of the coke beds can be controlled using a shape parameter, and their resistivity ranges between 4.12 mΩ·m and 7.20 mΩ·m. The model is coupled with an electrical circuit model that serves as the power supply, tracking the true power for each phase. However, structural elements surrounding the furnace are not incorporated in this model.

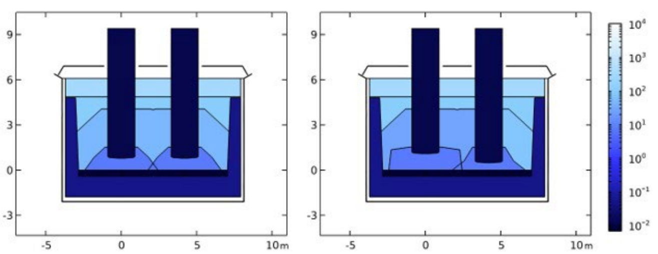

Figure 1—Cross section through the centres of electrode 3 and 1. The ideal case (left) and the unbalanced (right). Resistivity (mΩ·m) of the material is color coded, the darker the more conductive

The model is implemented in COMSOL Multiphysics (COMSOL Inc., 2024b) and Maxwell's equations are solved in the frequency domain using the magnetic and electric fields (mef) interface (COMSOL Inc., 2024a).

To study the Bøckman leads under different conditions, three reference cases have been considered, and the different parameters are listed in Table 1. In the "ideal" case, the electrode tips are equidistant from the alloy pool, and the shape factors and material properties of the coke beds are equal across all three electrodes. The left panel of Figure 1 illustrates the ideal case by showing the cross section passing through electrodes 3 and 1. For the "unbalanced" case, the electrodes have different heights within the coke beds, and these beds possess distinct characteristics such as shape, material properties, and surrounding conditions (right panel in Figure 1). In the "balanced" case, the properties of the coke beds and charges remain the same as in the unbalanced case, while electrode tip positions and the transformer voltages have been adjusted to achieve balanced electrical conditions and the correct power level.

The Bøckman method

The time-varying magnetic fields existing in the vicinity of the furnace due to the electrode currents give rise to induced voltages in the Bøckman leads. The voltage V_f^L at the end of the L-th lead can be calculated as the sum of the voltage at the starting point (V_i) and the induced term:

$$V_f^L = V_i + \int_L \frac{\partial \vec{A}}{\partial t} \cdot d\vec{l}, \qquad [1]$$

where $\partial \vec{A}/\partial t$ is the induced electric field, the integral is calculated as a path integral over L, and $(\partial \vec{A}/\partial t)\cdot\vec{l}$ is the component of the induced electric field tangential to the path L. The Bøckman

Table 1
Parameters defining the three cases

Case	Ideal	Unbalanced	Balanced
Root-mean-square transformer voltage (V)	250.00	250.00	246.00
Electrode 1 tip position (m)	0.80	0.50	0.74
Electrode 2 tip position (m)	0.80	0.80	1.04
Electrode 3 tip position (m)	0.80	1.10	1.13
Resistivity coke bed 1 (mΩ·m)	7.20	7.10	7.10
Resistivity coke bed 2 (mΩ·m)	7.20	6.50	6.50
Resistivity coke bed 3 (mΩ·m)	7.20	4.12	4.12
Coke bed 1 shape (1)	0.50	0.30	0.30
Coke bed 2 and 3 shape (1)	0.50	0.98	0.98
Resistivity charge el. 1 and 2 (mΩ·m)	47.00	72.08	72.08
Resistivity charge el. 2 and 3 (mΩ·m)	47.00	26.54	26.54
Resistivity charge el. 3 and 1 (mΩ·m)	47.00	26.54	26.54

method uses three measuring leads (L, M, and N). The voltage at the point at which these leads are connected is the average of the three lead voltages (V_f^L, V_f^M, and V_f^N):

$$V_f^{(LMN)} = \frac{1}{3}\left(V_f^L + V_f^M + V_f^N\right) = V_i + \frac{1}{3}\left(\int_L \frac{\partial \vec{A}}{\partial t}\cdot d\vec{l} + \int_M \frac{\partial \vec{A}}{\partial t}\cdot d\vec{l} + \int_N \frac{\partial \vec{A}}{\partial t}\cdot d\vec{l}\right).$$

In the ideal case, the induced voltages cancel and $V_f^{(LMN)}=V_i$.

The voltage induced in the Bøckman leads has the same frequency as the original time-varying magnetic field. Therefore, the voltage in the L-th lead can also be written as

$$V_f^L - V_i = A(L,P)\sin[\omega t + \phi(L,P)], \qquad [2]$$

where the amplitude $A(L,P)$ and phase $\phi(L,P)$ of the signal depend on the path of the lead (L) and the paths of the electric currents that generate the magnetic field in the first place (P). Regardless of the amplitude and phase, the sum of two or more sinusoidal waves with the same frequency ω is again a sinusoidal wave with frequency ω:

$$V_f^L - V_i = A_L\sin(\omega t + \phi_L),\quad V_f^M - V_i = A_M\sin(\omega t + \phi_M),\quad V_f^N - V_i = A_N\sin(\omega t + \phi_N)$$
$$3\left(V_f^{(LMN)} - V_i\right) = \sum_{i\in\{L,M,N\}} A_i\sin(\omega t + \phi_i) = A_{(LMN)}\sin\left(\omega t + \phi_{(LMN)}\right) \qquad [3]$$

where we have written A_i=$A(i,P)$ and ϕ_i=ϕ(i,P) for simplicity, and $A_{(LMN)}$ and ϕ_$_{(LMN)}$ satisfy

$$A_{(LMN)}^2 = \sum_{i,j} A_i A_j\cos(\phi_i - \phi_j),\quad \tan\phi_{(LMN)} = \frac{\sum_i A_i\sin\phi_i}{\sum_i A_i\cos\phi_i}, \qquad [4]$$

for $i \in \{L,M,N\}$ and $j \in \{L,M,N\}$. In real-world implementations of the Bøckman measurement, the positioning of leads in an industrial environment often involves negotiating obstacles and other equipment, resulting in a tortuous path. On the other hand, when conducting modelling investigations, ideal implementations tend to use straight segments for simplicity. Despite these differences, Equation 2 shows that both scenarios result in an induced voltage with a sinusoidal waveform and Equations. 3 and 4 show that values of the amplitudes A_i and phases ϕ_i exist for which $V_f(LMN) = V_i$.

The left panel of Figure 2 demonstrates two lead implementations: one that is curvilinear and another that is idealised and consists of four straight segments. Both paths originate beneath the alloy bath in the conductive carbon lining (this point will be referred to as the "hearth" in the remainder of the article) and terminate at the furnace's central axis 16 m above the alloy level. For reference, the straight path descends to a depth of 2 m below the furnace base and it remains 5 m away from the vertical wall of the steel shell. The segmented and curvilinear path lengths are 46.3 m and 57.5 m, respectively. These paths are colour-coded

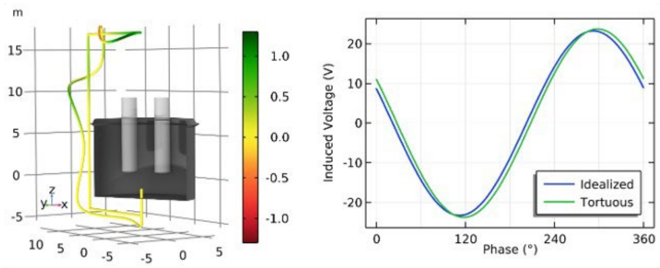

Figure 2—Left: A tortuous vs. an idealised lead color coded with the instantaneous amplitude of the tangential electric field (V/m). Right: corresponding sinusoidal signal of the induced voltage during a current cycle

based on the tangential component of the electric field (V/m), which integrates to yield the total induced voltage (Equation 1). The right panel of the figure illustrates the sinusoidal waveforms of the induced voltages over one cycle of the current. Interestingly, even for an overly tortuous path, the induced voltage can be well approximated by analysing the induced voltage in an ideal lead placed in the same general area. For this reason, the remainder of this work will focus on simplified straight paths.

Figure 3 shows the inner workings of the Bøckman system as intended in the original patent. The left panel shows the relationship between the time-resolved voltages during one current cycle, whereas the right panel shows the corresponding phasors. With the leads being symmetrically placed around the furnace, the phasors of the induced voltages point to the vertexes of an equilateral triangle centred at the origin. Consequently, the phasor sum cancels and the voltage at the common connection of the Bøckman leads is equal to the voltage in the hearth. (The deviation from zero in Figure 3 is a numerical artifact arising from asymmetries in the computational mesh.)

Ideal case

This section focuses on the ideal case, as outlined in Table 1. In the ideal case, the material distribution within the furnace has a three-fold rotational symmetry. Additionally, the electric circuit energising the system applies equal voltages to all electrodes. Under these conditions, the furnace exhibits a total active power of 38.9 MW and reactive power of 42.3 MVA. The electrode resistance is measured at 0.74 mΩ with a root-mean-square (RMS) current of 132.5 kA.

Symmetric lead placement

To investigate an idealised Bøckman system, the furnace model has been surrounded by 36 instances of the previously discussed idealised lead, spaced at intervals of 10°. Figure 4 shows a representation of these leads, colour-coded based on the tangential component of the electric field, at a specific moment within the current cycle. The FEM calculation shows that the contributions from each of the segments, constituting one lead, are in phase. Furthermore, owing to its length, the vertical segment is responsible for approximately 50% of the total induced voltage while the top section, where the lead returns toward the center, accounts for around 40%. The bottom horizontal section only contributes about 10% to the total signal, and the vertical section from the hearth downward has no contribution because it coincides with the symmetry axis of the furnace. Due to the idealised nature of these leads (only vertical and radial segments) the tangential component

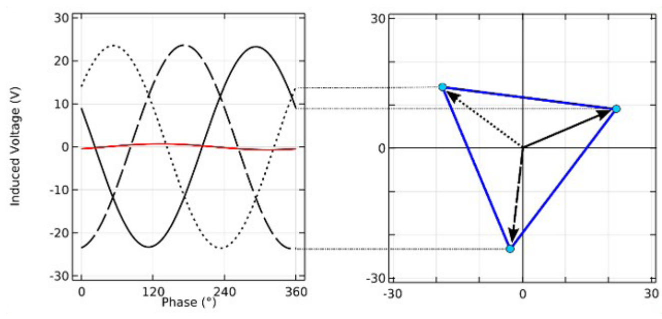

Figure 3—Time resolved and phasor diagram of the induced voltages in a three-leads symmetric Bøckman system in the eclipsed configuration. The combined signal of the three leads in red

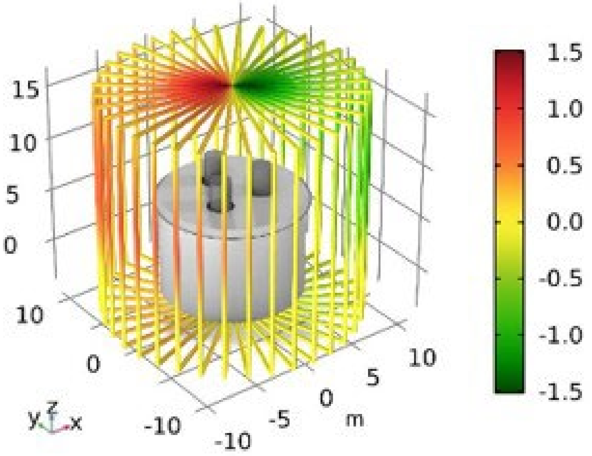

Figure 4—Symmetric furnace: 36 leads colour coded with the instantaneous amplitude of the tangential electric field (V/m)

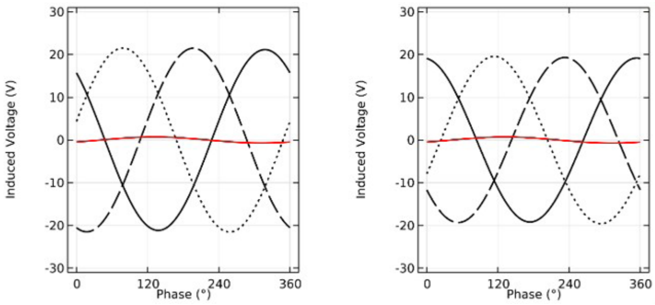

Figure 5—Two distinct implementations of the Bøckman method, based on leads in the staggered configuration (right) and a configuration that is intermediate between the fully eclipsed and staggered configurations (left). Both implementations give the same cancellation of the induced voltages (red lines)

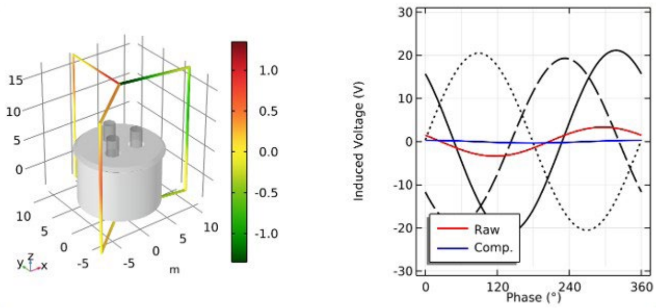

Figure 6—Asymmetry in the placement of the leads. Effect on the partial destructive interference (red) and compensated sum (blue)

of the electric field appears as a dipole structure rotating at the frequency of the current. The dipole symmetry can be understood by considering the analogy between the three-phase current in the three furnace electrodes and the current in a three-phase slot-wound dipole electric motor (Pyrhonen et al., 2014).

Supplementary Figure S-1 displays the time-resolved induced voltage for the 36 leads depicted in Figure 4. Due to the harmonic nature of the electromagnetic field surrounding the furnace, a geometric rotation of the leads around the furnace's center corresponds to a phase shift of a comparable angle. The amplitude of the induced signal depends on the positioning of the lead relative to the electrodes. For example, leads in an eclipsed configuration (positioned directly behind the electrodes) experience a larger induction compared to leads in a staggered configuration (positioned between the electrodes). The induced voltages are approximately 23.5 V and 19.0 V in the two cases.

Since a Bøckman system needs three measuring leads spaced 120° apart, the 36 leads depicted in Figure 4 enable the simulation of 12 unique Bøckman implementations. The induced voltages over one current cycle are shown in Figure 3 for leads in the eclipsed configuration and in Figure 5 for leads in the staggered and an in-between configuration. Symmetry considerations dictate that, in the ideal case, the induced voltages in the three Bøckman leads interfere destructively. The numerical experiments discussed in Figures 3 and 5 demonstrate that the FEM implementation is able to capture these effects with satisfying accuracy.

Asymmetric lead placement and compensation

Achieving perfect symmetry in lead placement is often challenging in an industrial setting. To address this, a strategy for compensating for asymmetric placement was developed as part of the original patent; an adjustable impedance can be used on each of the leads to ensure full cancellation (Bøckman, 1973a, 1973b).

Figure 6 investigates the impact of asymmetric placement of the leads on the implementation result. In this example, the leads are spaced at intervals of 130°, 140°, and 90°, instead of the standard 120°. Consequently, the destructive interference is only partial, and there is a residual induction error present after averaging the lead contributions (red line). In principle, there are an infinite number of possible ways to compensate the three signals so that their sum cancels (Equations 3 and 4).

Figure 7A provides an alternative representation, through a phasor diagram, of the partial destructive interference caused by the asymmetric leads mentioned above. The phasor summation reveals the presence of a residual induction error (depicted as solid red). In the real-world setup, the measurement error will be one third

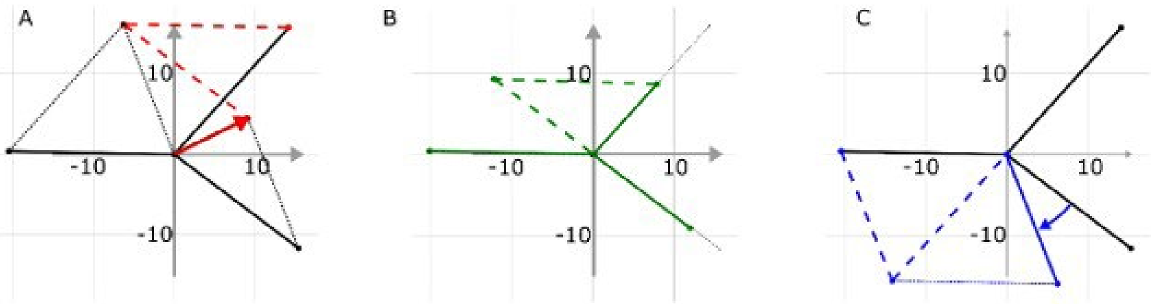

Figure 7—A: Phasor diagram of the induced voltage of a Bøckman system with asymmetric placement of the leads. B: Compensation by two resistances. C: Compensation by one impedance

of the sum due to averaging. Formally, two degrees of freedom are sufficient to bring the induction error to zero, i.e., two resistors or one resistor and one inductor/capacitor. Figure 7B demonstrates the simulation of an appropriate choice of two resistors to achieve compensation by scaling two of the three original phasors by 58% and 80%, respectively. The summation of these compensated phasors leads back to the origin of the coordinate system, indicating complete cancellation. Alternatively, Figure 7C presents another approach where the equivalent effect of a single impedance is applied to one of the leads. In this specific instance, the signal of the second lead is scaled to 89% and rotated by 31.5° (blue arrow).

The real-world compensation procedure has a significant impact on the quality of the hearth-voltage measurement. Errors in the calibration of the Bøckman resistors will affect the resulting measurements of the electrode voltages. Further investigation is needed to identify the optimal approach to compensation.

Unbalanced case

This section extends the analysis of Section 4 to cover the scenario of an unbalanced furnace by focusing on the unbalanced case outlined in Table 1 and Figure 1. In this case, the electrodes are positioned at distances of 50 cm, 80 cm, and 110 cm from the alloy bath. The resulting total active power is 38.8 MW, and the total reactive power is 46.5 MVA. The resistances of the electrodes are calculated to be 0.64 mΩ, 0.64 mΩ, and 0.70 mΩ, with RMS currents of 138.0 kA, 144.5 kA, and 137.2 kA, respectively.

Symmetric lead placement

With this furnace configuration, the three induced voltages have different amplitudes, and their phases are not spaced 120° apart. Consequently, there is only a partial destructive interference and a residual induction error is present in addition to the actual hearth voltage, as shown in Figure 8 for two different implementations. The left panels show leads in an eclipsed configuration, whereas the right panel show staggered leads. The similarities between the two implementations suggests that the residual inductive signal is independent of the lead path. In fact, the inductive error is identical across all 12 Bøckman implementations to an accuracy of 0.01 V of amplitude and 0.1° of phase. To conclude, despite the symmetric lead placement as described in the original patent, a residual inductive voltage persists in the unbalanced case. The residual induction error is more or less in phase with the true hearth voltage.

Asymmetric lead placement and compensation

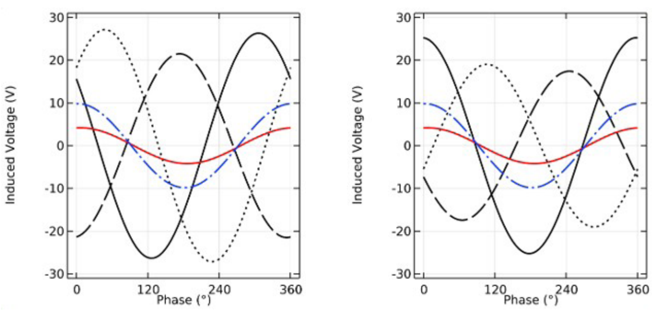

Figure 8—Unbalanced case with symmetric lead placement. Two distinct implementations of the Bøckman method, based on eclipsed (left) or staggered (right) leads. The combination of the three leads (black lines) gives partial cancellation of induced voltages (red lines). Voltage in the hearth of the furnace for reference (blue)

As demonstrated in Section 4, scaling and rotating a single phasor can effectively compensate for the effects of asymmetric lead placement in the ideal case. However, it remains to be determined if this compensation strategy retains its validity in non-ideal furnace environments. Figure 9 illustrates a Bøckman system with asymmetric lead placement in the unbalanced case. Asymmetric lead placement leads to a larger residual inductive error, and one that is phase shifted with respect to the case with symmetric leads. However, applying the same compensation as for the ideal case almost brings the inductive error back to the value seen for symmetric leads. To conclude, compensation for asymmetric lead placement works for unbalanced as well as ideal furnaces.

Balanced case

In the unbalanced case, there are significant differences among the three electrode resistances. This section considers the balanced case in Table 1, in which the electrodes' penetration into the burden has been changed to return all three electrode resistances to the interval 0.734 mΩ –0.737 mΩ, with RMS currents of 132.3 kA – 132.7 kA. Furthermore, the transformer voltage has been adjusted to achieve the same active power as in the previous cases (38.9 MW).

Despite achieving electrical balance, different voltages are still induced in the Bøckman leads due to the asymmetric distribution of materials in the furnace, which again leads to an asymmetric distribution of current within the furnace volume. Consequently, a residual inductive error persists. As shown in Figure 10, this error remains in phase with the voltage in the hearth. A comparison between Figure 8 and Figure 10 demonstrates that an electrical rebalancing of the furnace reduces both the residual inductive error in the Bøckman leads (from 4.2 V to 2.9 V), as well as the voltage in the furnace hearth (from 9.8 V to 4.6 V).

Conclusion

A 3D FEM model for the electrical conditions of a FeMn furnace has been implemented to study the induction in the leads used in the Bøckman system. In the scenario where the electrical state of the furnace is balanced, and the material distributions are

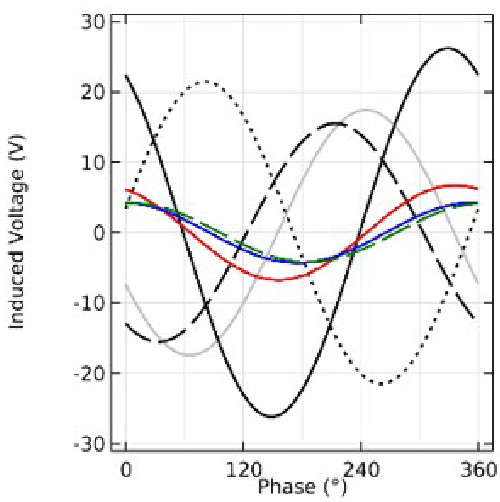

Figure 9—Unbalanced case with asymmetric lead placement. The uncompensated voltages in the leads are shown as gray (solid) and black (solid and dotted) lines. The compensated voltage in one of the leads is shown as a black dashed line. The uncompensated induction error is shown in red. The compensated induction error is shown in blue, to be compared with a symmetric lead placement (green)

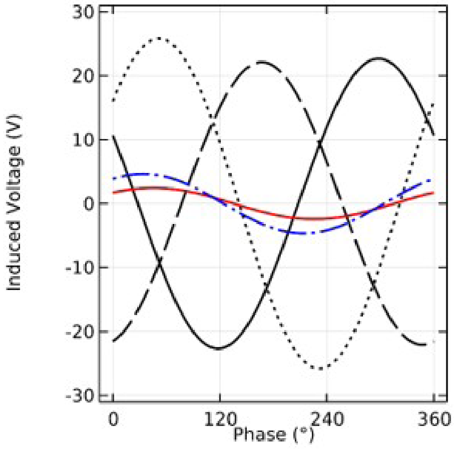

Figure 10—Balanced case with symmetric lead placement. The combination of the three Bøckman leads (black lines) gives partial cancellation of induced voltages (red line). Voltage in the hearth of the furnace for reference (blue)

symmetric, placing the leads symmetrically around the furnace permits complete destructive interference of the induced voltage. Conversely, in a situation with material imbalances in the furnace, only partial cancellation of signals occurs, leading to a residual induction error. Notably, the residual voltage is in phase with the voltage in the hearth, thus not interfering with the electrode controllers. Rebalancing the electrodes of a furnace with an asymmetric material distribution reduces the residual induced voltage, but cannot eliminate it entirely.

An asymmetric placement of the Bøckman leads must be compensated for to achieve a cancellation of the induced voltages. Compensation can be achieved using at least two resistors or one resistor and one inductor/capacitor, and the compensation remains valid irrespective of the furnace state.

Acknowledgements

This paper is published as part of the project "Electrical Conditions in Submerged Arc Furnaces—Identification and Improvement" (SAFECI), with financial support from the Research Council of Norway (project number 326802) and the companies Elkem, Eramet Norway, Finnfjord and Wacker Chemicals Norway.

Author statement

MS: Conceptualisation, methodology, software, investigation, formal analysis, writing – original draft preparation, visualisation, project administration, funding acquisition.

VKR: Conceptualisation, methodology, formal analysis, writing – original draft preparation, writing – review and editing preparation.

UT: Methodology, formal analysis, writing – original draft preparation.

Conflict of interest

The authors declare that they have no conflict of interest.

Bibliography

Bezuidenhout, J.J., Eksteen, J.J., Bradshaw, S.M. 2009. Computational fluid dynamic modelling of an electric furnace used in the smelting of PGM containing concentrates. Minerals Engineering, vol. 22, no. 11, pp. 995–1006. Available at: https://doi.org/10.1016/j.mineng.2009.03.009

Bøckman, O.C. 1973a. Anordning for måling av kraterspenningene i en trefase smelteovn med elektrodene i trekant. Available at: https://patents.google.com/patent/NO126288B/en

Bøckman, O.C. 1973b. Arrangement for measuring the crater voltages in a three-phase electric furnace with electrodes arranged in a delta. Available at: https://patents.google.com/patent/US3757021/en

COMSOL Inc. 2024a. AC/DC module user's guide. v6.2. Available at: https://doc.comsol.com/6.2/doc/com.comsol.help.acdc/ACDCModuleUsersGuide.pdf

COMSOL Inc. 2024b. COMSOL multiphysics reference manual. v6.2. Available at: https://doc.comsol.com/6.2/doc/com.comsol.help.comsol/COMSOL_ReferenceManual.pdf

Darmana, D., Olsen, J.E., Tang, K., Ringdalen, E. 2012. Modeling concept for submerged-arc furnaces. *Proceedings of the 9th International Conference on CFD in the Minerals and Process Industries. CSIRO, Melbourne, Australia*. Available at: https://www.cfd.com.au/cfd_conf12/PDFs/062DAR.pdf

Dhainaut, M. 2004. Simulation of the electric field in a submerged arc furnace. *Proceedings of the 10th International Ferro-Alloys Congress (INFACON X). South African Institute of Mining and Metallurgy, Cape Town, South Africa*, pp. 605–613. Available at: https://www.pyrometallurgy.co.za/InfaconX/079.pdf

Fromreide, M., Gómez, D., Halvorsen, S.A., Salgado, P. 2023. Induced currents in the lining and steel shell of submerged arc furnaces. *Journal of Sustainable Metallurgy*, vol. 9, no. 1, pp. 375–385. Available at: https://doi.org/10.1007/s40831-022-00625-6

Fromreide, M., Halvorsen, S.A., Sparta, M., Risinggård, V.K., Salgado, P., Gómez, D., Herland, E.V. 2021. Effects of alternating currents in the hearth of submerged arc furnaces. *Proceedings of the 16th International Ferro-Alloys Congress (INFACON XVI). Social Science Research Network, Trondheim, Norway.* Available at: https://doi.org/10.2139/ssrn.3926716

Gerritsen, T., Tracy, P., Saber, F. 2015. Electrode voltage measurement in electric furnaces: Analysis of error in measurement and calculation. *Proceedings of the 14th International Ferro-Alloys Congress (INFACON XIV). International Committee on Ferro-Alloys, Kyiv, Ukraine*, pp. 338–348. Available at: https://www.pyrometallurgy.co.za/InfaconXIV/338-Gerritsen.pdf

Halvorsen, S.A., Olsen, H.A.H., Fromreide, M. 2016. An efficient simulation method for current and power distribution in 3-phase electrical smelting furnaces. *IFAC-PapersOnLine*, vol. 49, no. 20, pp. 167–172. Available at: https://doi.org/10.1016/j.ifacol.2016.10.115

Herland, E.V., Sparta, M., Halvorsen, S.A. 2018. 3D models of proximity effects in large FeSi and FeMn furnaces. Journal of the Southern African Institute of Mining and Metallurgy, vol. 118, no. 6, pp. 607–618. Available at: https://doi.org/10.17159/2411-9717/2018/v118n6a8

Herland, E.V., Sparta, M., Halvorsen, S.A. 2019. Skin and proximity effects in electrodes and furnace shells. Metallurgical and Materials Transactions B, vol. 50, no. 6, pp. 2884–2897. Available at: https://doi.org/10.1007/s11663-019-01651-8

Karalis, K., Karalis, N., Karkalos, N., Ntallis, N., Antipas, G.S.E., Xenidis, A. 2021. Three-dimensional computational fluid dynamics analysis of an electric submerged arc furnace. *Scientific Reports*, vol. 11, no. 1, pp. 17637. Available at: https://doi.org/10.1038/s41598-021-96085-1

Karalis, K.T., Karkalos, N., Cheimarios, N., Antipas, G.S.E., Xenidis, A., Boudouvis, A.G. 2016. A CFD analysis of slag properties, electrode shape and immersion depth effects on electric submerged arc furnace heating in ferronickel processing. *Applied Mathematical Modelling*, vol. 40, no. 21–22, pp. 9052–9066. Available at: https://doi.org/10.1016/j.apm.2016.05.045

Magnussen, T.E. 2018. Basic parameters in the operation and design of submerged arc furnaces, with particular reference to production of high-silicon alloys. J*ournal of the Southern African Institute of Mining and Metallurgy*, vol. 118, no. 6. Available at: https://doi.org/10.17159/2411-9717/2018/v118n6a11

Pyrhonen, J., Jokinen, T., Hrabovcová, V. 2014. Design of rotating electrical machines. 2nd ed. Wiley.

Scheepers, E., Yang, Y., Adema, A.T., Boom, R., Reuter, M.A. 2010. Process modeling and optimization of a submerged arc furnace for phosphorus production. *Metallurgical and Materials Transactions B*, vol. 41, no. 5, pp. 990–1005. Available at: https://doi.org/10.1007/s11663-010-9403-3

Sparta, M., Varagnolo, D., Martens, H., Halvorsen, S.A. 2021. Metamodeling of the electrical conditions in submerged arc furnaces. Proceedings of the 16th International Ferro-Alloys Congress (INFACON XVI). Social Science Research Network, *Trondheim*. Available at: https://doi.org/10.2139/ssrn.3926715

Sparta, M., Varagnolo, D., Stråbø, K., Halvorsen, S.A., Herland, E.V., Martens, H. 2021. Metamodeling of the electrical conditions in submerged-arc furnaces. Metallurgical and Materials Transactions B, vol. 52, pp. 1267–1278. Available at: https://doi.org/10.1007/s11663-021-02089-7

Stewart, A.B. 1980. An analysis of the electrical circuit of submerged-arc furnaces. PhD thesis. University of Cape Town. Available at: http://hdl.handle.net/11427/14048

Tesfahunegn, Y.A., Magnússon, Þ., Tangstad, M., Sævarsdóttir, G.A. 2018a. Effect of electrode shape on the current distribution in submerged arc furnaces for silicon production – a modelling approach. *Journal of the Southern African Institute of Mining and Metallurgy*, vol. 118, no. 6, pp. 595–600. Available at: https://doi.org/10.17159/2411-9717/2018/v118n6a6

Tesfahunegn, Y.A., Magnússon, Þ., Tangstad, M., Sævarsdóttir, G.A. 2018b. The effect of pitch circle diameter of electrodes on current distributions in submerged arc furnace. 2018 *IEEE MTT-S International Conference on Numerical Electromagnetic and Multiphysics Modeling and Optimization (NEMO). IEEE, Reykjavík, Iceland.* Available at: https://doi.org/10.1109/NEMO.2018.8503177

Tesfahunegn, Y.A., Magnússon, Þ., Tangstad, M., Sævarsdóttir, G.A. 2020a. Comparative study of AC and DC solvers based on current and power distributions in a submerged arc furnace. *Metallurgical and Materials Transactions* B, vol. 51, no. 2, pp. 510–518. Available at: https://doi.org/10.1007/s11663-020-01794-z

Tesfahunegn, Y.A., Magnússon, Þ., Tangstad, M., Sævarsdóttir, G.A. 2020b. The effect of side arcs on current distributions in a submerged arc furnace for silicon production. J. Lee, S. Wagstaff, G. Lambotte, A. Allanore, and F. Tesfaye (eds.). Materials Processing Fundamentals 2020. *The Minerals, Metals & Materials Series, Springer International Publishing*, pp. 177–188. Available at: https://doi.org/10.1007/978-3-030-36556-1_16

Tesfahunegn, Y.A., Magnússon, Þ., Tangstad, M., Sævarsdóttir, G.A. 2021. The effect of electrode movements on electrical characteristics of a submerged arc furnace. JOM, vol. 73, no. 10, pp. 2963–2972. Available at: https://doi.org/10.1007/s11837-021-04818-4

Tesfahunegn, Y.A., Sævarsdóttir, G.A., Magnússon, Þ., Tangstad, M. 2018. The effect of frequency on current distributions inside submerged arc furnace. *2018 IEEE MTT-S International Conference on Numerical Electromagnetic and Multiphysics Modeling and Optimization (NEMO)*. IEEE, Reykjavík, Iceland. Available at: https://doi.org/10.1109/NEMO.2018.8503083

Toh, T., Yamasaki, N., Seki, T., Tanaka, J. 2005. Magnetohydrodynamic simulation in steelmaking process by 3D finite volume method. *Proceeding of the 4th International Conference on CFD in the Minerals and Process Industries. SINTEF Academic Press, Trondheim*, Norway. Available at: https://www.sintef.no/globalassets/project/cfd2008/cfd2005_papers/21_toh_yamasaki_seki_tanaka.pdf

Yu, Y., Li, B., Liu, Z., Qi, F., Liu, C., Rong, W., Kuang, S. 2023. Simulation of ferrochrome settling behavior in a submerged arc furnace using a multiphysics and multiphase model. *Metallurgical and Materials Transactions B*, vol. 54, no. 4, pp. 2080–2094. Available at: https://doi.org/10.1007/s11663-023-02817-1

Yu, Y., Li, B., Yun, C., Qi, F., Liu, Z. 2021. Modeling on reduction reaction of metal oxides for submerged arc furnace in ferrochrome pellets smelting process. *Metallurgical and Materials Transactions B*, vol. 52, no. 6, pp. 3907–3919. Available at: https://doi.org/10.1007/s11663-021-02304-5

Zienkiewicz, O.C., Morgan, K. 2006. Finite elements and approximation. Dover Publications. ◆

SOUTHERN AFRICAN MINE WATER CONFERENCE 2026

LET'S CONNECT

VENUE – GLENBURN LODGE AND SPA, MULDERSDRIFT
15 NOVEMBER 2026 – TECHNICAL WORKSHOPS
16 -17 NOVEMBER 2026 – TECHNICAL CONFERENCE
18 NOVEMBER 2026 – TECHNICAL VISIT

In Partnership:

ECSA and SACNASP Validated CPD Activity Credits = 0.1 per hour attended

SAIMM THE SOUTHERN AFRICAN INSTITUTE OF MINING AND METALLURGY

ABOUT THE CONFERENCE

The Southern African Institute of Mining and Metallurgy (SAIMM), in collaboration with the International Mine Water Association (IMWA), the Mine Water Division of the Water Institute of Southern Africa (WISA-MWD) and Mintek, warmly invites you to the Southern African Mine Water Conference 2026, a premier gathering where science, technology and sustainability intersect.

Guided by the theme "Let's Connect," this conference is more than an event – it's a movement to bridge disciplines, foster innovation and build resilient solutions for mine water management. Attendees will explore a wide spectrum of topics, from the complexity of mine water geochemistry to the transformative power of AI-driven modelling and simulation.

Discover how mining-influenced water (MIW) can be repurposed through circularity and value recovery and gain insights into the latest advancements in water treatment technologies and microbial processes that are reshaping environmental stewardship.

Whether you are a researcher, engineer, policymaker or industry practitioner, this is your chance to engage with cutting-edge developments, share your expertise and help shape a more connected future for mine water innovation.

CONFERENCE TOPICS

Explore cutting-edge developments and share insights on:

- Mine water geochemistry
- Utilisation of mining-influenced water (MIW), circularity and recovery of value products
- Modelling and simulation
- Artificial Intelligence applications
- Water treatment technologies
- Microbial processes in mine water systems

CALL FOR PAPERS/ PRESENTATIONS

Prospective authors are invited to submit short abstracts of not more than 500 words. Abstracts should consist of 4 paragraphs describing the presentation's relevance, the methods used, the key results and their application as well as implications.

Authors of accepted abstracts will be required to submit a full paper for peer review and publication in the conference proceedings. A presentation only option will be considered.

KEY DATES

21 May 2026 – Submission of abstracts
27 June 2026 – Submission of papers

SUBMIT AN ABSTRACT

FOR FURTHER INFORMATION, CONTACT:

Gugu Charlie,
Conferences and Events Coordinator

E-mail: gugu@saimm.co.za
Tel: +27 11 530 0238
Web: www.saimm.co.za